Pertanika J. Sci. & Technol. 30 (1): 35 - 52 (2022)

PERTANIKA JOURNALS

SCIENCE & TECHNOLOGY

Journal homepage: http://www.pertanika.upm.edu.my/

Multi-band Antenna with CSRR Loaded Ground Plane and Stubs Incorporated Patch for WiMAX/WLAN Applications

Palanivel Manikandan[1]*, Pothiraj Sivakumar[1] and Nagarajan Rajini[2]

[1]*Department of Electronics and Communication Engineering, Kalasalingam Academy of Research and Education, Tamilnadu-626126, India*
[2]*Department of Mechanical Engineering, Kalasalingam Academy of Research and Education, Tamilnadu-626126, India*

ABSTRACT

This paper proposes a novel compact, single structure, multi-band antenna along with tested results for wireless local area networks (WLAN) and Worldwide Interoperability for Microwave Access (WiMAX) applications. In this work, modified complementary split-ring resonators (CSRR) were incorporated in the ground layer of the patch to achieve permeable bands to accommodate multi-resonance frequencies in a single device. The proposed antenna design supported the upgraded performance and led to desirable size reduction. Open stubs were incorporated at the edges of the triangle batch to get the improved reflection coefficient responses. It resulted in specific band spectra of 2.4 / 3.4 / 5.1 / 5.8GHz for WLAN/WiMAX applications. For constructive antenna design, CST microwave studio simulation software was utilized. S_{11} parameter was observed as -24dB at 2.4GHZ, -32dB at 3.4GHz. -15dB at 5.1GHz and -22dB at 5.8GHz bands. Field patterns of each band were observed. The parametric study of the arrangement and positioning of the CSRR unit cell was examined. Excellent consistency between the experimental and simulated results revealed the capability of the projected structure to perform with improved gain.

Keywords: CSRR, microstrip, multi-band antenna, WiMAX, WLAN

ARTICLE INFO

Article history:
Received: 12 May 2021
Accepted: 15 September 2021
Published: 06 December 2021

DOI: https://doi.org/10.47836/pjst.30.1.03

E-mail addresses:
maanip85@gmail.com (Palanivel Manikandan)
sivapothi@gmail.com (Pothiraj Sivakumar)
rajiniklu@gmail.com (Nagarajan Rajini)
* Corresponding author

INTRODUCTION

Today's wireless communication systems focus on the enhancement of current techniques using multi-band antennas. The features of multi-band antennas include compact size, low cost, easy fabrication, multiple resonating frequencies, less weight, and low profile (Ali et al., 2018). The

ISSN: 0128-7680
e-ISSN: 2231-8526

advantages of microstrip antennas are easy accommodation with compact devices due to their planar structure, low profile, less weight, and easy integration with circuits. These features make them highly suitable for communication devices. Developments in the microstrip antenna domain and an increase in the demands of microstrip antennas are transforming the field of communication technology (Peixeiro, 2011). However, microstrip antennas have a few limitations, such as narrowband resonance and poor efficiency. Hence, many techniques were later developed to overcome these limitations (Wong, 2002; Waterhouse, 2003). The performance of microstrip-patch antennas was improved by implementing a cavity structure on the back of the patch with many dielectric layers and shorts. In addition, fractal structures were implemented to provide wideband characteristics (Rahim et al., 2019). Multi-band technique for wireless applications can be achieved by incorporating slots over structures (Zavosh & Aberle, 1996), fractal geometries (Baliarda, 1998), stubs at various locations (Ali & Biradar, 2017), multi-layered structures (Firdausi & Alaydrus, 2016), reconfigurable structures (Sung, 2014), aperture coupling feed, feeding techniques (Casula et al., 2016), insertion of parasitic elements, electronically reconfiguring the antenna using microelectronic switches (Parchin et al., 2020) or by making defected ground structures (DGS). Multi-band antenna is reported in slotted rectangular patch antenna for wireless applications (Malik & Singh 2019).

Recent developments in wireless communications demand multiple bands in the range of 6 to 100 GHz (Ishfaq et al.,2017). In 5G wireless technology, antennas for mobile or other handheld electronic devices are compact and demand operation in multi-resonance frequency bands (Cheng et al., 2020). For ease of fabrication, planar antennas are desirable, while bandwidth limitations can be overcome by following techniques such as incorporating slots in the radiating elements (Zong et al., 2015), metamaterials (Xu et al., 2012; Xu et al., 2013), and making defects in the ground plane (Chiang & Tam, 2008). Many antennas designed using complementary split-ring resonators (CSRR) were allocated for gain and bandwidth enhancement (Ntaikos et al., 2011). CSRR is a unique structure to produce a very firm magnetic field coupling on the source of EM Field than by using conventional materials (Liu et al., 2013). It reduces the geometrical size of the antenna without modifying its properties (Dong & Itoh, 2011; Dong et al., 2012). Multi-band antenna was developed through fractal structure and CSRR based ground plane (Manikandan et al., 2020). A compact dual-band antenna for high-frequency wireless applications was reported (Erentok & Ziolkowski, 2008). A microstrip multi-band antenna was proposed by loading an SRR with slots to miniaturize the structure (Sarkar et al., 2014). Wi-Fi and WiMAX applications can be achieved through CSRR with radiating elements (Nelaturi & Sarma, 2018) through miniaturizing characteristics (Ntaikos et al., 2011) and adaptive frequency reconfigurability (Manikandan et al., 2019). Finding the dimension of an antenna can be done with the help of design equations. However, there is a need to optimize the element's dimensions

or feed to ensure improved results. Currently, many optimization methods exist. Genetic algorithms and evolution stratégies were applied to find the dimensions of horn antenna for good results (Deepika et al., 2017). Challenges in designing a 5G communication system antenna to fulfill multi-band requirements were reported (Shaik & Malik, 2021).

This paper presents a multi-band triangular antenna using CSRR with four bands, i.e., 2.4 /3.4 / 5.1 / 5.8 GHz for WLANand WiMAX applications. CSSR was introduced on the ground layer of the microstrip to realize the additional bands without making physical changes in the patch. Metallic open stubs were incorporated to shift the existing bands to the desired multi-resonant frequencies with improved reflection coefficients. In this work, a microstrip triangular patch was examined with and without CSRR. A computer simulation technology (CST) software tool was appropriated to design and simulate the constructed antenna. It showed high radiation features at distinct frequencies, making our proposal the correct element for WLAN and WiMAX applications.

METHODS

Design of Triangular Patch

The proposed multi-band antenna was designed and fabricated over a commercially available FR4 substrate with a dielectric constant of 4.4, thickness value of 1.60 mm, and loss tangent of 0.02. The designed multi-band antenna had dimensions of 30 mm x 25.98 mm with a 50 Ohm transmission line. An equilateral triangular shape patch was considered because it required less metal area on the substrate compared to existing regular shapes like a rectangle or circle (Garg & Long, 1988). Based on the literature, the dimensions of an equilateral triangle were considered as per Equation 1 for 2.75GHz, which was radiated due to the fringing fields of the patch and simulated with CST microwave studio simulation software.

$$a = \frac{2c}{3f_r\sqrt{\varepsilon_r}} \qquad [1]$$

Where, a = side length of the equilateral triangle
f_r = resonance frequency
ε_r = Relative dielectric constant of the substrate used

The triangular patch dimension is considered for 3 GHz. The antenna progressed in numerous stages to attain multi-resonance frequencies by adjusting its parameters. After introducing the large slots on the base sides of the triangle, a fully grounded patch provided two resonance frequencies, such as 2.75 and 4.5GHz, due to effective surface current distribution at a different place at each resonance. At the lower resonance frequency, the maximum surface current is distributed at the center area of the triangle and minimum at the parallel edges. At higher resonance, maximum surface current existed at edges and

the minimum at the center. A microstrip feed was matched with a patch radiator, having a selected dimension of 15 mm and 2.5 mm, respectively. Esteemed reference impedance was 50 ohm. The antenna was fabricated with the dimensions specified in Figure 1.

The proposed triangle was fed with the microstrip feed as an impedance matching transformer to give 50 ohms matching the load. The dimensions of the radiating element are given in Table 1.

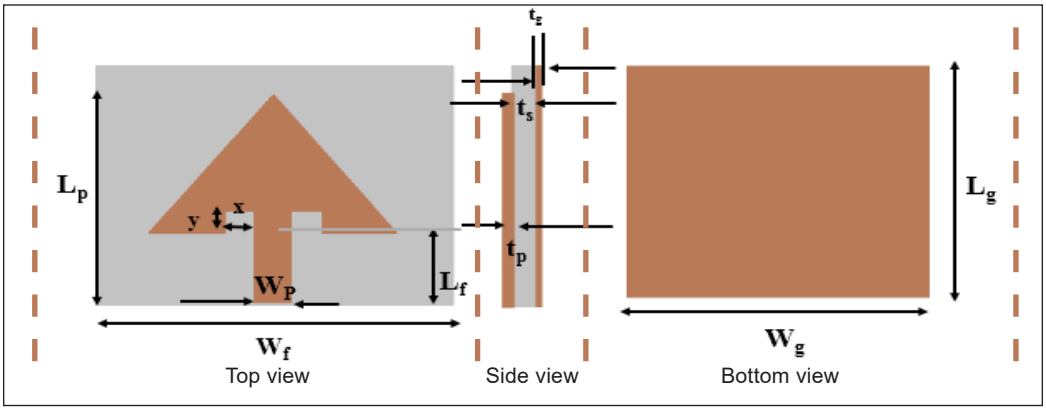

Figure 1. Geometrical parameters of the triangle patch

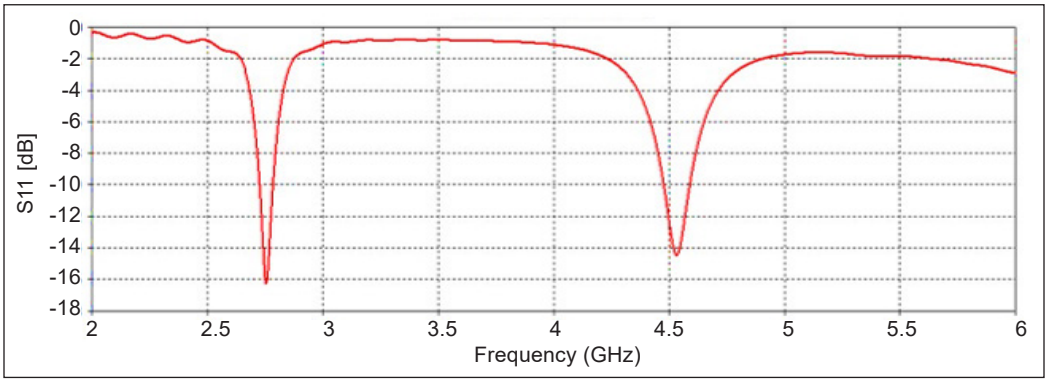

Figure 2. Simulation result of S11 versus frequency

Table 1
Dimensions of the triangle patch

Antenna	
Parameters	**Value**
Dimensions of patch ($W_p \times L_p \times t_p$)	$30 \times 25.98 \times 0.035 mm^3$
Dimensions of slot (x × y)	$15 \times 7.5\ mm^2$
Dimensions of feed ($W_f \times L_f$)	$2.5 \times 30\ mm^2$
Dimensions of ground ($W_g \times Lg \times tg$)	$60 \times 60 \times 0.035\ mm^3$
Thickness of the substrate (t_s)	1.6 mm

Figure 1 displays the geometrical parameters, and Figure 2 is the graph of the reflection coefficient (S11 in dB) of the proposed multi-band triangle. The prescribed triangle provided a very minimal S11 response at the frequencies of 2.75 and 4.5GHz.

Introducing Complementary Slip Ring Resonator on Ground Layer

The complementary split-ring resonator (CSRR) was incorporated into the ground side of the triangle patch antenna. The capacitive nature of CSRR created an electric field when energized. This electric field created an electromotive force (EMF) in CSRR, which generated fluctuating voltage among the slots of CSRR at RF frequencies. The dimensions and the equivalent circuit model of CSRR are given in Figure 3. The boundaries were altered to obtain unit cell scattering parameters. As a result, the appearance of TEM wave broadcasts was in the direction of the y-axis. The E-field of the incident wave was oriented along the direction of the z-axis, and the H-field in the direction of the x-axis, as shown in Figure 4. The effect of proposed resonators can be exhibited on a microstrip patch by promoting the circuit model of the CSRR. Further reduction in the dimensions of these

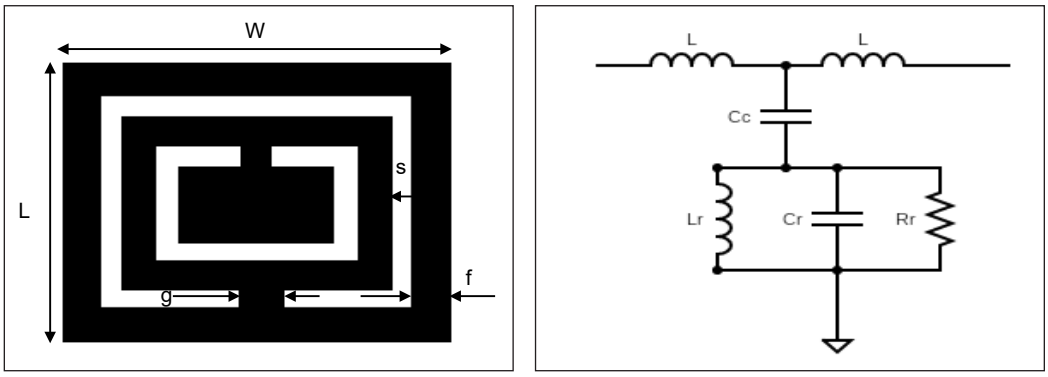

(a) (b)

Figure 3. (a) Dimensions; and (b) Equivalent circuit of CSRR

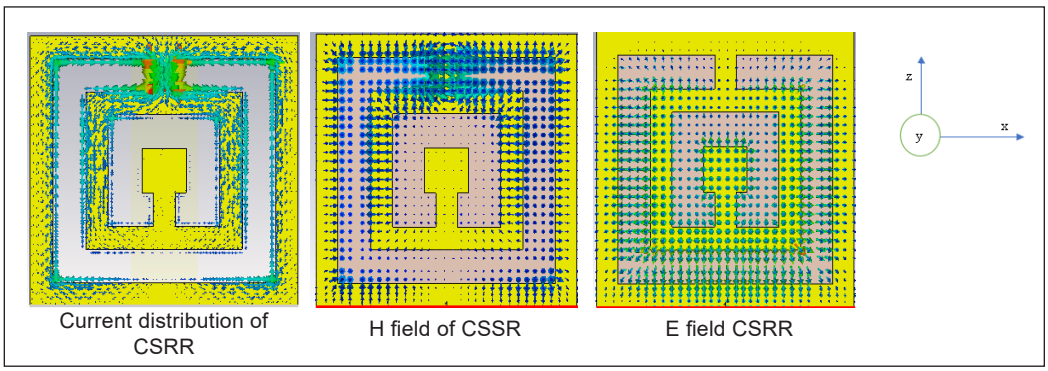

Figure 4. (a) Current distribution; (b) H field; and (c) E field of CSRR

artificial transmission lines was executed through a single cell. Mutual capacitance existed through the electric field in the gap between the conductor of CSRR, and inductance was established due to the current flow across the transmission line. Thus, CSRR acted as a resonance circuit with the parallel Rr, Lr, and Cr resonating structures, as shown in Figure 3(b).

Analysis of the Location of CSRR Incorporated Over a Ground Plane

Table 2 demonstrates the dimensions of CSRR to be loaded. In Figure 3, the designed CSRR was loaded with the proposed patch to attain a multi-band resonance (Aminu-Baba et al., 2018). L represents the inductance of the lines in CSRR. The latter was described through the resonators and designed with the parallel R_r, L_r, and C_r coupled with the host Conductor, as presented by coupling capacitance C_c. When the dielectric losses were insignificant (based on the 1st order approximation), Multi-resonance was realized with a patch, as shown in Figure 6. It demonstrated the S parameter characteristics of the projected patch with a CSRR incorporated ground plane. Experimentally, it confirmed that it could radiate at 2.45GHz with S11 equal to –34 dB and 4.5 GHz with S11 equal to –10 dB. Thus, it was significant for WLAN applications. The developed element was a type of CSRR used in this design and etched into the ground layer of the patch, as shown in Figure 5.

Table 2
Optimal dimensions of CSRR

CSRR	
Parameters	Value (mm)
Length (L)	7
Width (W)	7
Width of metal (f)	1
Spacing (s)	0.7
Width of metal strip connected ring (g)	0.3

Figure 5 demonstrates the suitably positioned CSRR in the ground layer, touching the vertical axis o at the rear of the feed line attached to the proposed patch. This portion determined the positioning of the rectangular unit cell without changing the dimensions.

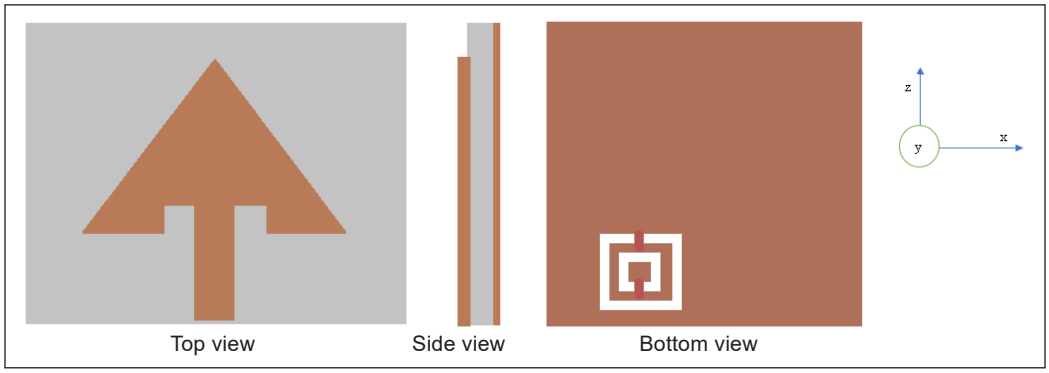

Figure 5. Proposed multi-band triangle with CSRR on the ground plane

The rectangular unit cell that emerged at the patch was positioned with the ground layer, symmetric to the feed of the maximum field to achieve a lower level in the patch.

The rectangular CSRR was placed in the X-direction, -3.5 mm from the feed center and 7 mm from the feed edge in the Y-direction. Thus, the left corner of the CSRR was precisely under the feed line. This positioning of the CSRR made the antenna resonates effectively in a lower band frequency of 2.45 GHz. Furthermore, the results revealed that the acceptable reflection coefficient transpired at the first band itself, as shown in Figure 6.

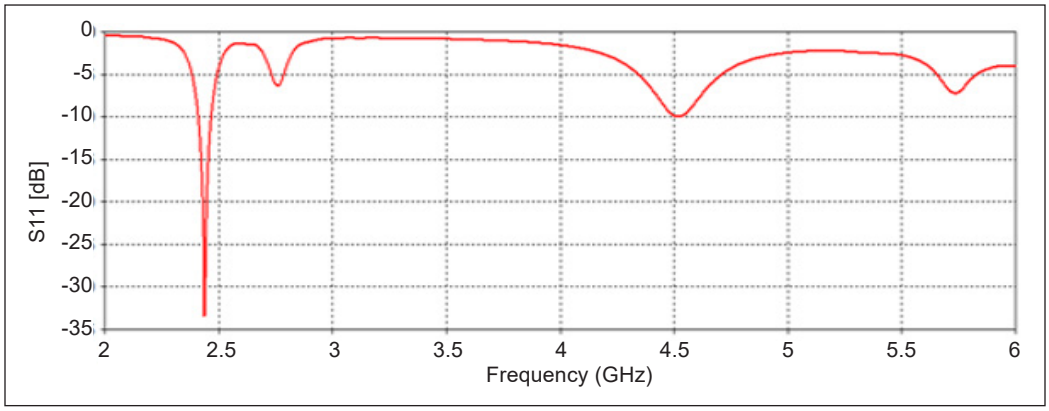

Figure 6. Simulated S11 response of patch with CSRR incorporated ground plane

Introduction of Stubs to the Edges of the Patch

Stubs were incorporated at the edges of the proposed CSRR loaded patch antenna to shift the frequencies with adequate reflection coefficient value (Deshmukh & Tirodkar, 2013; Deshmukh et al., 2012). When the length of stub was in the order of one by a fourth of the wavelength, it gave different capacitive and inductive reactance in various resonance frequencies of the antenna and accomplished frequency shift with a significant reflection coefficient. Stubs were introduced on the patch edges to alter the current distribution and improve frequency response at 2.4, 3.4, 5.1, and 5.8GHz. We have made a study on stub length to exhibit better performance. When the stub length was increased, surface current flow direction was associated more in the x-direction, the radiation pattern developed was normal to the surface of the patch. Also, cross-polarization levels were eliminated. By varying stub length, surface current distribution, and radiation pattern direction were different to get the significant reflection coefficient. The impedance of the stubs has changed the impedance of the patch at each resonance.

Thus, the open circuit stub altered the frequency of the proposed patch element. As a result, the formulated element of the multi-band triangle shown in Figure 7 was expected to get multiple bands corresponding to one of the wireless applications at 2.4 / 3.4 /5.1 / 5.8 GHz.

The radiating frequency of the patch excluding CSRR was achieved at 2.75 and 4.5 GHz. Incorporating a CSRR under the patch in the ground plane offers significant resonance at 2.45 and 4.5GHz. In Table 3, the comparison analysis shows that CSRR has brought the two new resonance frequencies at 2.45 GHz and 5.7GHz. However, most of the remaining bands having poor reflection coefficient responses other than 2.45GHz.

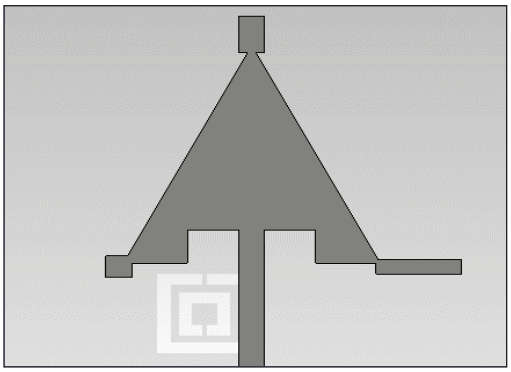

Figure 7. Patch with extended stub on the edges and the CSRR incorporated ground plane

Table 3
Comparison analysis

	Resonance frequency (GHz)	Reflection Coefficient (dB)
Triangle patch without CSRR and stubs	2.75	-16
	4.5	-14
Patch with CSRR incorporated ground plane	2.45	-34
	2.75	-06
	4.5	-10
	5.7	-07
Patch with stubs and CSSR incorporated ground plane	2.4	-24.5
	3.4	-34
	5.1	-16
	5.8	-23

CSSR grounded patch with stubs have provided the shift on the resonance frequencies of the patch with good reflection coefficient values.

Optimization

Optimization of various parameters was undertaken to make the obtained frequency bands suitable for wireless applications with enough S11 value. By adjusting the feed width, input impedance was made to resemble an improved reflection coefficient ideally. The width of the feed line was optimized by the Tree-seed Optimization algorithm (Kiran, 2015).

Tree-seed Algorithm for Feed width Optimization. This algorithm was implemented as per the following steps:

Step 1: Initial feed width value was calculated from the transmission line equation and was considered the initial Tree location. New feed width values were calculated by using Equation 2,

$$W_{x,y} = L_{y,min} + r_{x,y}(H_{y,max} - L_{y,min}) \quad [2]$$

Where $L_{y,max}$ is the Lower value of the feed width.
$H_{y,max}$ is the Upper value of the feed width.
$r_{x,y}$ is the Scaling factor randomly selected between 0 and 0.1.

Step 2: The best solution was obtained from populated values (Equation 3).

$$B_y = min\{f(W_x)\} \quad [3]$$

where x=0, 1, 2, 3, 4…N
N is the number of feed width values in the search range.

Step 3: If the best Optimized feed width was not obtained, New feed width could be considered as per the following Equations 4 and 5

$$S_{xy} = T_{xy} + \alpha_{x,y} * (B_y - T_{r,y}) \quad [4]$$

$$S_{xy} = T_{xy} + \alpha_{i,j} * (T_{x,y} - T_{r,y}) \quad [5]$$

Where;
S_{xy} is the y-th dimension of x-th feed width that would be produced at i^{th}impedance.
T_{xy} is the y-th dimension of x-th impedance,
B_y is the y-th dimension of the obtained feed width.
$T_{r,y}$ is the y-th dimension of r^{th} impedance randomly chosen from the population.
$a_{x,y}$ is the scaling factor randomly selected in a range of -0.1 to 0.1.

The selection of new feed width was controlled by the patch impedance parameter called Searching Tendency (ST), and its value was in a range of 0 to 0.1.

Step 4: The above steps were repeated until the best seed was obtained or an iteration value of 100.

The feed width dimension was optimized according to the steps specified in the flowchart shown in Figure 8. The best feed width values of sample iterations are listed in Table 4. Feed width of 2.9 mm was the optimized value to realize better reflection coefficient S11(dB) for the proposed structure.

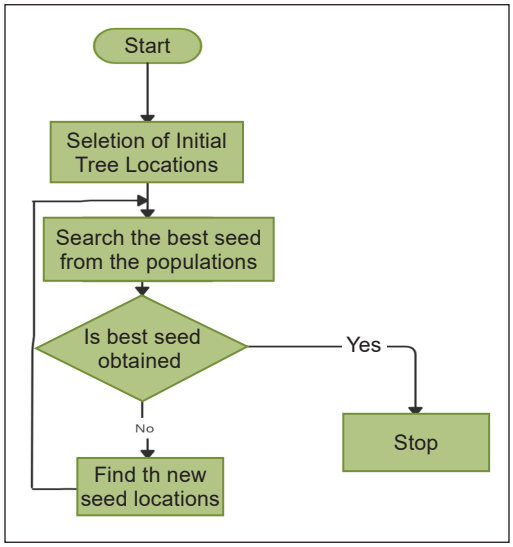

Figure 8. Flow chart of the Tree-Seed Optimization Algorithm

Table 4
Optimized feed width of sample iterations

Sample Iteration	Optimized Feed width value (mm)	S11 (dB) for different frequency bands		
		2.4 GHz	3.4 GHz	5.8GHz
1	2	-11.03	-22.12	-27.5
2	2.5	-14.858	-24.576	-23.36
3	2.7	-17.02	-17.47	-28.7
4	2.8	-19.37	-26.33	-29.738
5	2.9	-24.485	-33.843	-23.102
6	3.1	-20.9	-12.5	-18

Figure 9 shows the fabricated antenna. The element was fabricated using a commercially available FR4 substrate and loaded with a CSRR incorporated ground layer. The element was attached to the SMA connector to measure the radiating characteristics.

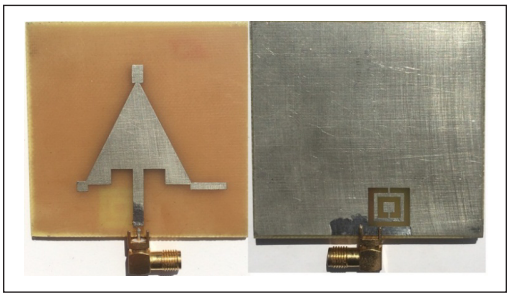

Figure 9. Photograph of fabricated stub incorporated CSRR loaded multiband antenna

RESULTS AND DISCUSSION

Reflection Coefficient

The designed technique showed sustained results that matched the simulated results. However, the simulated and measured S11 of the projected element varied slightly. It was noted that the developed prototype radiated at 2.4 / 3.4 / 5.1 / 5.8 GHz, respectively.

Due to the placement of the rectangular unit cell near the SMA connector, it was observed that there was a minor change in the reflection coefficient, which affected the antenna's radiating properties. The experimental results of S11 (in dB) are plotted in Figure 10. It was observed that the frequencies matched precisely. However, the reflection

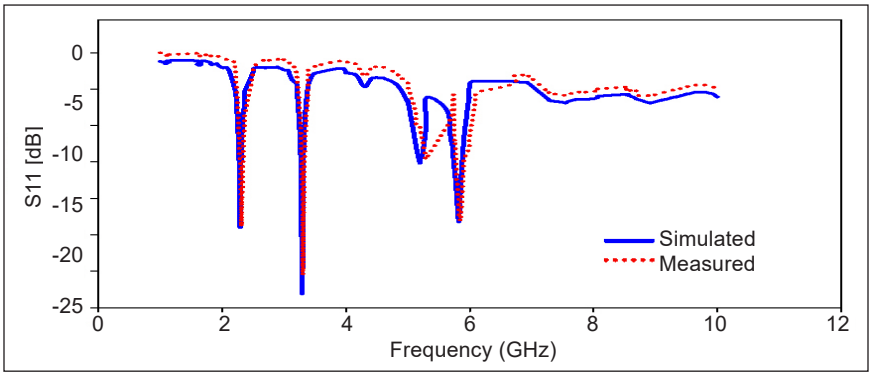

Figure 10. Simulated and measured S11 response

Table 5
Comparison between simulated and experimental results

Parameters	Frequency band (GHz)	S_{11} Parameter (dB)	Gain (dB)	Efficiency (dB)
Simulated	2.4	-24.5	4.38	-2.85
	3.4	-34	3.46	-3.21
	5.1	-16	1.98	-4.06
	5.8	-23	4.7	-2.53
Measured	2.4	-24	4.25	-2.98
	3.4	-32	3.12	-3.5
	5.1	-15	1.52	-4.2
	5.8	-22	4.58	-2.82

coefficient of the simulated and the measured values varied slightly due to setup limitations like connector loss, excessive soldering and sharp edges in the slots, fabrication tolerances, and improper impedance matching of the driving source for optimum power transfer. The comparison values are tabulated in Table 5.

From the graph in Figure 10, the proposed antenna ensured better performance and was superior compared to existing antennas from literature.

Gain and Efficiency

Predictable values of gain and efficiency were realized for each resonant frequency. The proposed antenna radiated at 2.4, 3.4, 5.1, and 5.8 GHz with a gain of 4.38, 3.46, 1.28, and 4.79 dB, respectively. The measured gain and efficiency values for each resonance frequency were closely matched with the simulation results, as shown in Table 5. The smaller distance between CSRR and the SMA connector provided excellent gain improvement at 2.4 GHz.

Radiation Pattern

Figure 11 represents three-dimensional simulated radiation patterns of the projected antenna observed using simulation software. Simulated radiation patterns clearly showed that the patch radiated normal at its plane for all resonance frequencies. However, the shape of the patterns differed slightly among all resonances due to different surface current distributions at each resonance frequency.

Figure 12 demonstrates the measured and simulated radiation patterns for E-Plane and H-plane at 2.4 / 3.4 / 5.1 / 5.8 GHz. Again, the measured and simulated patterns were closely matched. H Plane pattern was observed for all theta values (0 to 360 degrees) by keeping constant phi=90 degrees. E Plane pattern was observed for all theta values (0 to 360 degrees) by keeping constant Phi=0 degree.

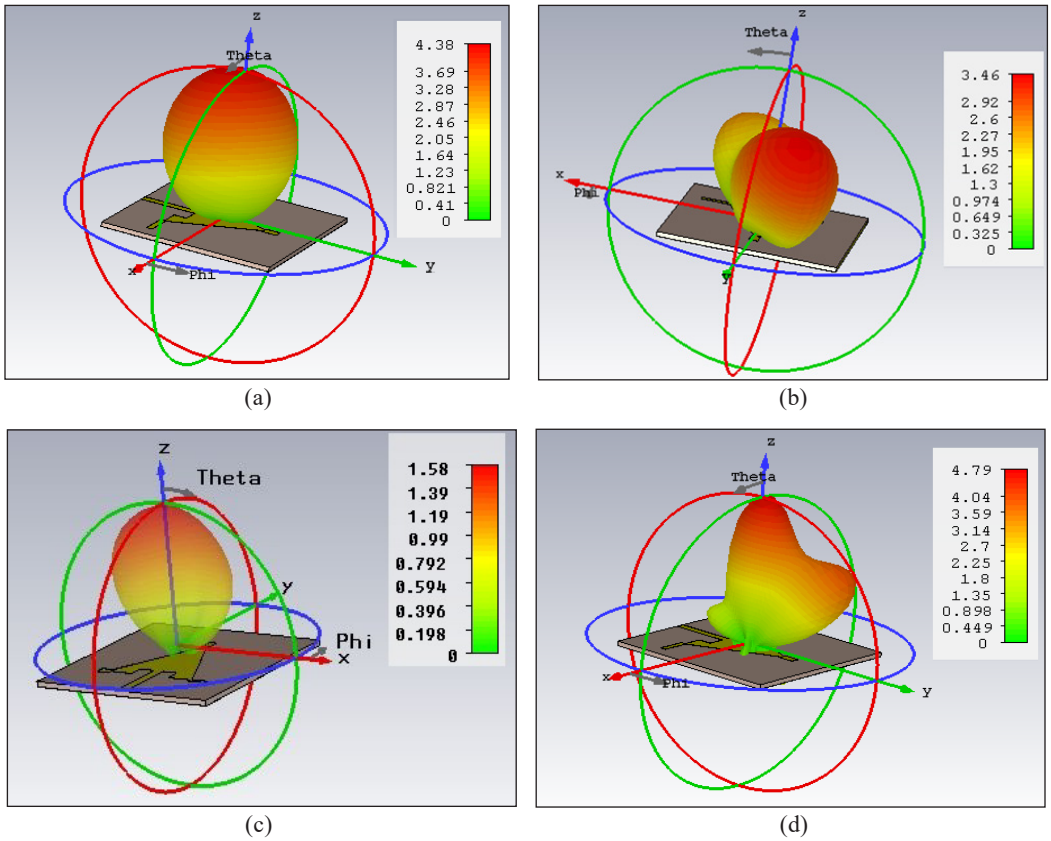

Figure 11. Simulated 3D radiation patterns of (a) 2.4 GHz, (b) 3.4 GHz, (c) 5.1 GHz and (d) 5.8 GHz

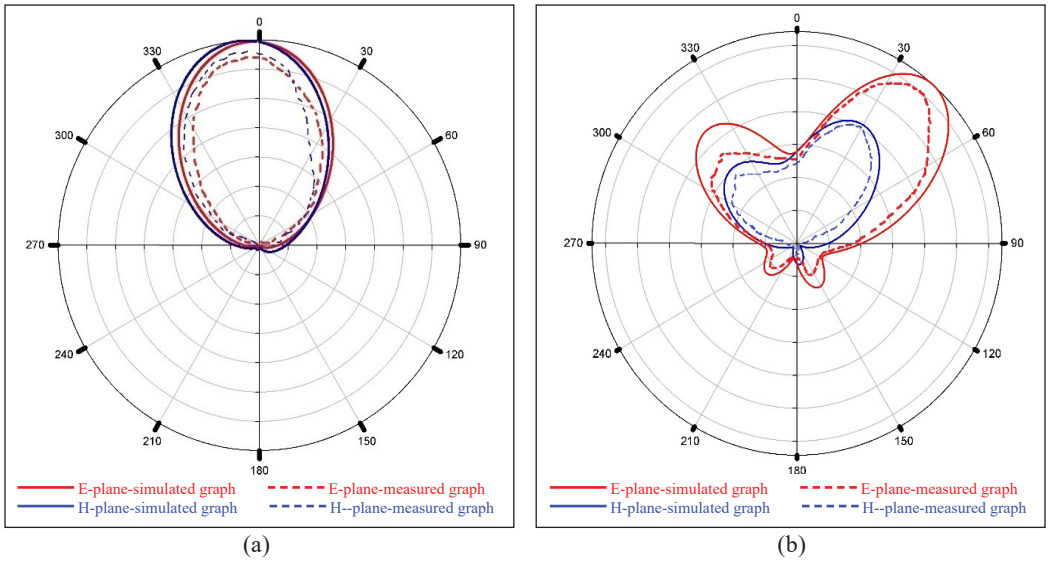

Figure 12. Practical and simulation patterns of (a) 2.4GHz, (b) 3.4GHz, (c) 5.1GHz and (d) 5.8GHz

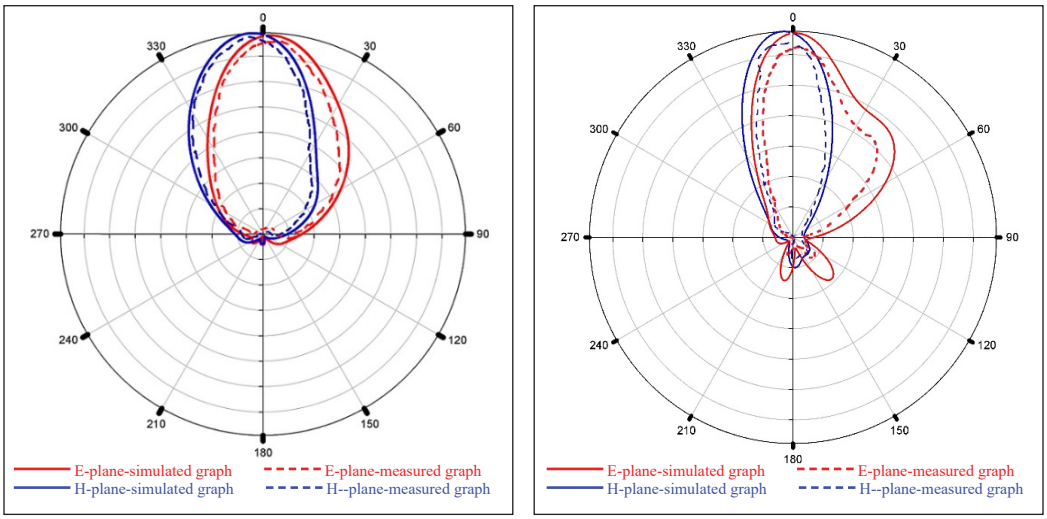

Figure 12 (continue). Practical and simulation patterns of (a) 2.4GHz, (b) 3.4GHz, (c) 5.1GHz and (d) 5.8GHz

Surface Current Distribution

The surface current distribution of the proposed antenna for each resonance frequency is shown in Figure 13. The following Figure 13 represents the exact current path of the designed antenna. Generally, the resonance frequency of radiation depends on the electrical length of the antenna. Therefore, the current travels in different paths at each resonance frequency, and the structure allows the appropriate current to provide effective radiation.

At the resonance frequency of 2.4 GHz, an appropriate current distribution existed on the sides of the patch, as shown in Figure 13(a). The current phase was reversed at each stub (edges of the patch), while the current direction did not change on each side and provided a low-frequency resonance. At 3.4 GHz frequency, significant current distribution was found at the junction between stubs and the top edge and on the right edge of the patch, as reported in Figure 13(b). The current phase was reversed at the middle of each side of the triangle as frequency and wavelength are inversely proportional to each other. Hence with an increase in the frequency, the length of the wave decreased, and the phase of the current changed in a shorter distance.

Figure 13(c) shows the current distribution of the antenna at 5.1 GHz. A strong current distribution existed on the edge of the patch, and the phase of the current changed by 180 degrees at every1/3 part of the patch's length formed by side length and stub length. At the resonance frequency of 5.8 GHz, the current phase changed thrice by 180 degrees over the length formed by side length and stub length, as shown in Figure 13(d).

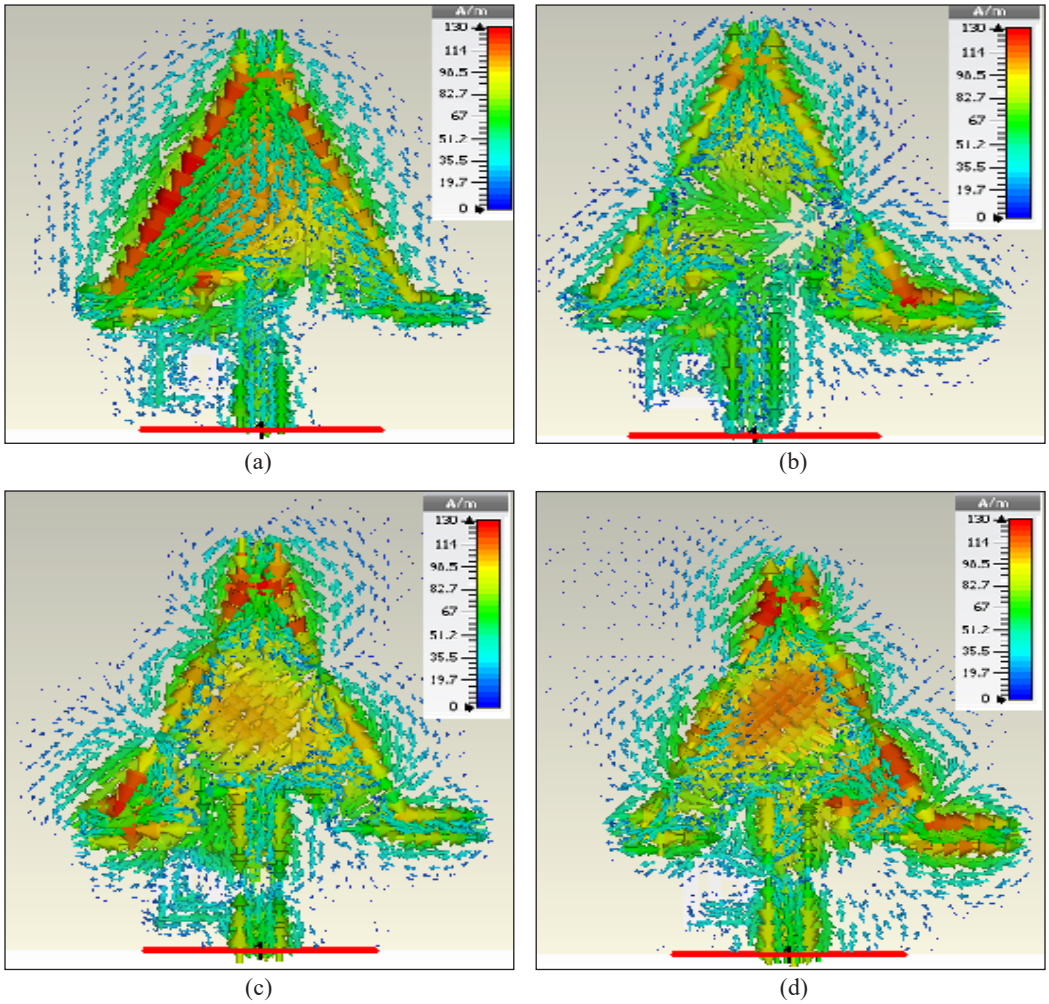

Figure 13. Surface current distribution at (a) 2.4 GHz, (b) 3.4 GHz, (c) 5.1 GHz and (d) 5.8 GHz

VSWR (Voltage Standing Wave Ratio)

VSWR denotes the power delivered to the antenna from the applied power source. Practical antennas require VSWR values ≤ 2. The proposed antenna reported a VSWR value between 1 and 2 at all four resonance frequencies, as shown in Figure 14. Thus, it ensured that more than 90% of the applied power was delivered to the antenna.

Input Impedance

The proposed antenna offered a 50-ohm input impedance for all resonance frequencies (2.4 / 3.4 / 5.1 / 5.8 GHz), as shown in Figure 15. Thus, the antenna received maximum power from the appropriate source connected through a 50-ohm connector.

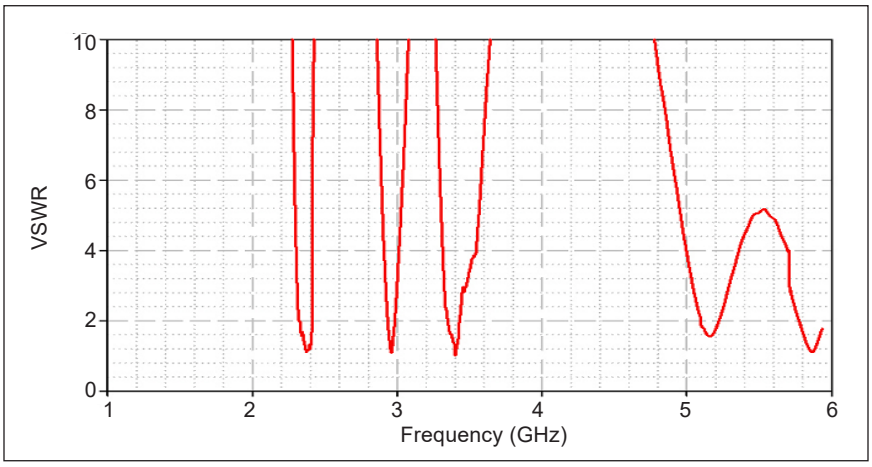

Figure 14. VSWR graph

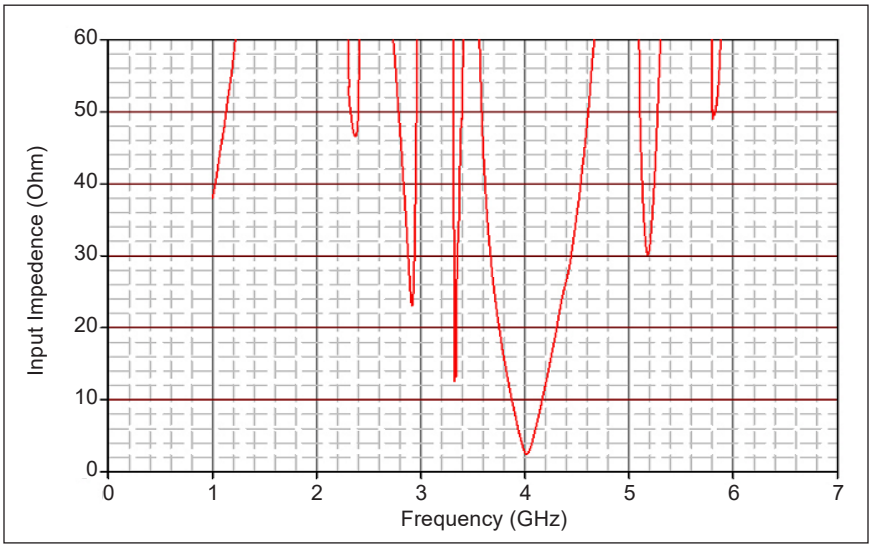

Figure 15. Input impedance graph

CONCLUSION

A novel CSRR loaded, stub-based microstrip triangle patch antenna for wireless application was proposed and fabricated in this study. As confirmed through simulation and measured results, the proposed antenna design was an authentic novel design for a multi-band microstrip antenna. The proposed antenna provided the reflection coefficient as -24dB at 2.4GHZ, -32dB at 3.4GHz. -15dB at 5.1GHz and -22dB at 5.8GHz bands. It was observed that the proposed triangle had a functional bandwidth of about 4.33, 3.03, 4.87, and 8.24% at resonance frequencies of 2.4, 3.4, 5.1, and 5.8 GHz, respectively. It provided a gain of 4.25, 3.12, 1.52, and 4.58 dB at resonance frequencies of 2.4, 3.4, 5.1, and 5.8 GHz,

respectively, and thus satisfied the demand for WLAN/WiMAX applications. The projected antenna revealed good E and H plane radiation characteristics. The design also provided a substantial size reduction, making it possible for the antenna to be placed in a single handheld wireless device to operate at four different resonant frequencies. The productive design was simulated using CST Microwave Studio and compared with experimental results. Both results were validated and showed that this antenna was much compact for use in wireless communication systems.

ACKNOWLEDGEMENT

The authors are thankful to the management of Kalasalingam Academy of Research and Education (KARE) for providing lab facilities during this research.

REFERENCES

Ali, T., & Biradar, R. C. (2017). A compact multiband antenna using λ/4 rectangular stub loaded with metamaterial for IEEE 802.11 N and IEEE 802.16 E. *Microwave and Optical Technology Letters, 59*(5), 1000-1006. https://doi.org/10.1002/mop.30454.

Ali, T., Pathan, S., & Biradar, R. C. (2018). Multiband, frequency reconfigurable, and metamaterial antennas design techniques: Present and future research directions. *Internet Technology Letters, 1*(6), Article e19. https://doi.org/10.1002/itl2.19

Aminu-Baba, M., Rahim, M. K. A., Zubir, F., & Yusoff, M. F. M. (2018). Design of miniaturized multiband patch antenna using CSRR for WLAN/WiMAX applications. *TELKOMNIKA Telecommunication, Computing, Electronics and Control*, *16*(4), 1838-1845.

Baliarda, C. P. (1998). On the behavior of the Sierpinski multiband fractal antenna. *IEEE Transactions on Antennas and Propagation, 46*(4), 517-524. https://doi.org/10.1109/8.664115

Casula, G. A., Maxia, P., Montisci, G., Valente, G., Mazzarella, G., &Pisanu, T. (2016). A multiband proximity-coupled-fed flexible microstrip antenna for wireless systems. *International Journal of Antennas and Propagation, 2016*, Article 8536058. https://doi.org/10.1155/2016/8536058

Cheng, Y., Lu, J., & Sheng, B. Q. (2020). MIMO handset antenna for 5G/WLAN applications. *Frontiers of Information Technology & Electronic Engineering, 21*(1), 182-187. https://doi.org/10.1631/FITEE.1900478

Chiang, K. H., & Tam, K. W. (2008). Microstrip monopole antenna with enhanced bandwidth using defected ground structure. *IEEE Antennas and Wireless Propagation Letters, 7*, 532-535. https://doi.org/10.1109/LAWP.2008.2005592

Deepika, R., Manikandan, P., & Sivakumar, P. (2017). Optimization of pyramid horn antenna using genetic algorithm and evolution strategy. In 2017 *IEEE International Conference on Electrical, Instrumentation and Communication Engineering (ICEICE)* (pp. 1-4). IEEE Publishing. https://doi.org/10.1109/ICEICE.2017.8191862.

Deshmukh, A. A., & Tirodkar, T. (2013). Formulation of Resonant Length for Triple Band Slot Cut Stub Loaded Rectangular Microstrip Antenna. *International Journal of Computer Applications, 975-8887*, 23-27.

Deshmukh, A. A., Pranali, S., Nikita, G., Monika, K., & Ray, K. P. (2012). Analysis of stub loaded equilateral triangular microstrip antennas. In *2012 International Conference on Communication, Information & Computing Technology (ICCICT)* (pp. 1-5). IEEE Publishing. https://doi.org/10.1109/ICCICT.2012.6398154

Dong, Y., & Itoh, T. (2012). Metamaterial-based antennas. *Proceedings of the IEEE, 100*(7), 2271-2285. https://doi.org/10.1109/JPROC.2012.2187631

Dong, Y., Toyao, H., & Itoh, T. (2011). Design and characterization of miniaturized patch antennas loaded with complementary split-ring resonators. *IEEE Transactions on Antennas and Propagation, 60*(2), 772-785. https://doi.org/10.1109/TAP.2011.2173120

Erentok, A., & Ziolkowski, R. W. (2008). Metamaterial-inspired efficient electrically small antennas. *IEEE Transactions on Antennas and Propagation, 56*(3), 691-707. https://doi.org/10.1109/TAP.2008.916949

Firdausi, A., & Alaydrus, M. (2016). Designing multiband multilayered microstrip antenna for mm Wave applications. In *2016 International Conference on Radar, Antenna, Microwave, Electronics, and Telecommunications (ICRAMET)* (pp. 99-102). IEEE Publishing. https://doi.org/10.1109/ICRAMET.2016.7849591

Garg, R., & Long, S. A. (1988). An improved formula for the resonant frequencies of the triangular microstrip patch antenna. *IEEE Transactions on Antennas and Propagation, 36*(4), 570. https://doi.org/10.1109/8.1148

Ishfaq, M. K., Rahman, T. A., Chattha, H. T., & Rehman, M. U. (2017). Multiband split-ring resonator based planar inverted-F antenna for 5G applications. *International Journal of Antennas and Propagation, 2017*, Article 5148083. https://doi.org/10.1155/2017/5148083

Kiran, M. S. (2015). TSA: Tree-seed algorithm for continuous optimization. *Expert Systems with Applications, 42*(19), 6686-6698. https://doi.org/10.1016/j.eswa.2015.04.055

Liu, J., Cheng, Y., Nie, Y., & Gong, R. (2013). Metamaterial extends microstrip antenna. *Microwaves & RF, 52*(12), 69-73.

Malik, P. K., & Singh, M. (2019). Multiple bandwidth design of micro strip antenna for future wireless communication. *International Journal of Recent Technology and Engineering, 8*(2), 5135-5138. https://doi.org/10.35940/ijrte.B2871.078219.

Manikandan, P., Sivakumar, P., & Swedheetha, C. (2019). Design of adaptive frequency reconfigurable antenna for MIMO applications. In *Soft Computing in Data Analytics* (pp. 203-213). Springer. https://doi.org/10.1007/978-981-13-0514-6_21

Manikandan, P., Sivakumar, P., Krishna, K. S. V., Sumanth, P., & Poornesh, T. (2020). A fractal based CSRR loaded multi-band antenna for wireless applications. *International Journal of Advanced Science and Technology, 29*(7s), 4486-4492.

Nelaturi, S., & Sarma, N. V. S. N. (2018). CSRR based patch antenna for Wi-Fi and WiMAX applications. *Advanced Electromagnetics, 7*(3), 40-45. https://doi.org/10.7716/aem.v7i3.700

Ntaikos, D. K., Bourgis, N. K., & Yioultsis, T. V. (2011). Metamaterial-based electrically small multiband planar monopole antennas. *IEEE Antennas and Wireless Propagation Letters, 10*, 963-966. https://doi.org/10.1109/LAWP.2011.2167309

Parchin, N. O., Basherlou, H. J., Al-Yasir, Y. I. A., Abdulkhaleq, A. M., & Abd-Alhameed, R. A. (2020). Reconfigurable antennas: Switching techniques - A survey. *Electronics, 9*(2), Article 336. https://doi.org/10.3390/electronics9020336

Peixeiro C. (2011). Microstrip patch antennas: An historical perspective of the development. In *2011 SBMO/ IEEE MTT-S International Microwave and Optoelectronics Conference (IMOC 2011)* (pp. 684-688). IEEE Publishing. https://doi.org/10.1109/IMOC.2011.6169224.

Rahim, A., Malik, P. K., & Ponnapalli, V. A. S. (2019). Fractal antenna design for overtaking on highways in 5g vehicular communication ad-hoc networks environment. *International Journal of Engineering and Advanced Technology, 9*(1S6), 157-160. https://doi.org/10.35940/ijeat.A1031.1291S619

Sarkar, D., Saurav, K., & Srivastava, K. V. (2014). Multi-band microstrip-fed slot antenna loaded with split-ring resonator. *Electronics Letters, 50*(21), 1498-1500. https://doi.org/10.1049/el.2014.2625.

Shaik, N., & Malik, P. K. (2021). A comprehensive survey 5G wireless communication systems: Open issues, research challenges, channel estimation, multi carrier modulation and 5G applications. *Multimedia Tools and Applications, 80*, 28789-28827. https://doi.org/10.1007/s11042-021-11128-z

Sung, Y. (2014). Multi-band reconfigurable antenna for mobile handset applications. *IET Microwaves, Antennas & Propagation, 8*(11), 864-871. https://doi.org/10.1049/iet-map.2013.0525

Waterhouse, R. B. (2003). Improving the efficiency of microstrip patch antennas. In *Microstrip Patch Antennas: A Designer's Guide* (pp. 167-195). Springer. https://doi.org/10.1007/978-1-4757-3791-2_4

Wong, K. L. (2002). *Compact and broadband microstrip antennas*. Jon Wiley & Sons. Inc.

Xu, H. X., Wang, G. M., Lv, Y. Y., Qi, M. Q., Gao. X., & Ge, S. (2013). Multifrequency monopole antennas by loading metamaterial transmission lines with dual-shunt branch circuit. *Progress in Electromagnetics Research, 137*, 703-725. http://dx.doi.org/10.2528/PIER12122409

Xu, H. X., Wang, G. M., Qi, M. Q., Zhang, C. X., Liang, J. G., Gong, J. Q., & Zhou, Y. C. (2012). Analysis and design of two-dimensional resonant-type composite right/left-handed transmission lines with compact gain-enhanced resonant antennas. *IEEE Transactions on Antennas and Propagation, 61*(2), 735-747. https://doi.org/10.1109/TAP.2012.2215298

Zavosh, F., & Aberle, J. T. (1996). Improving the performance of microstrip-patch antennas. *IEEE Antennas and Propagation Magazine, 38*(4), 7-12. https://doi.org/10.1109/74.537361.

Zong, W. H., Yang, X. M., Li, S. D., Wei, X. Y., &Hou, J. C. (2015). Design and fabrication of a wideband slot antenna for Handset Applications. In 2015 *IEEE International RF and Microwave Conference (RFM)* (pp. 161-165). IEEE Publishing. https://doi.org/10.1109/RFM.2015.7587735